

# Enhanced sensing response of solid-electrolyte gas sensors to toluene: Role of composite Au/metal oxide sensing electrode

Taro Ueda<sup>1</sup>, Hironari Abe<sup>1</sup>, Kai Kamada<sup>1</sup>, Sean R. Bishop<sup>2,§</sup>, Harry L. Tuller<sup>2,3</sup>, Takeo Hyodo<sup>1</sup> and Yasuhiro Shimizu<sup>1</sup>

<sup>1</sup>Graduate School of Engineering, Nagasaki University,  
1-14 Bunkyo-machi, Nagasaki 852-8521, Japan

<sup>2</sup>Department of Materials Science and Engineering, Massachusetts Institute of Technology,  
77 Massachusetts Avenue, Cambridge, Massachusetts 02139, USA

<sup>3</sup>International Institute of Carbon Neutral Energy Research, Kyushu University,  
744 Motooka, Nishi-ku, Fukuoka 819-0395, Japan

\*Corresponding author:

Taro Ueda, Dr.

Graduate School of Engineering, Nagasaki University

1-14 Bunkyo-machi, Nagasaki 852-8521, Japan

Tel: +81-95-819-2645

Fax: +81-95-819-2643

E-mail: taroueda@nagasaki-u.ac.jp

§ Present address: Redox Power Systems, College Park, MD 20742 USA

## **Highlights**

1. The YSZ-based sensor using CeO<sub>2</sub>-mixed Au SE showed good response to toluene.
2. The recovery time decreased with the addition of metal oxides to Au SE.
3. The toluene-sensing properties are largely dependent on the microstructure as well as catalytic and electrocatalytic activities.
4. The response increased with increasing toluene concentration (0.5–50 ppm).

## Abstract

In this study, YSZ-based potentiometric gas sensors of the type Au\*/YSZ/Pt, where Au\* represents either dense (d-Au), porous Au (p-Au) or porous Au/4MO<sub>x</sub> (4 wt% CeO<sub>2</sub>, Gd<sub>2</sub>O<sub>3</sub>, La<sub>2</sub>O<sub>3</sub>, Pr<sub>6</sub>O<sub>11</sub>, Sm<sub>2</sub>O<sub>3</sub>, Pr<sub>0.1</sub>Ce<sub>0.9</sub>O<sub>2</sub> or Ce<sub>0.8</sub>Zr<sub>0.2</sub>O<sub>2</sub>) composite sensor electrodes (SEs), were fabricated, and their toluene-sensing properties examined over the temperature range of 400–500°C. The roles of microstructure of the SEs, and improvements in sensing properties due to MO additions were examined with respect to their impact on catalytically enhanced toluene oxidation as well as electrochemical reactions at the SE/electrolyte interface. Au(4MO)/Pt sensors showed larger response to toluene than d-Au/Pt, with the Au(4CeO<sub>2</sub>)/Pt sensor showing the largest response among all of the Au(4MO)/Pt sensors. While the response of Au(4CeO<sub>2</sub>)/Pt was smaller than that of p-Au/Pt, its recovery time was much shorter. These observations were shown to result from Au(4CeO<sub>2</sub>) exhibiting the largest catalytic activity of toluene oxidation among all of the oxides tested, leading to enhanced toluene oxidization during its diffusion through the SE, as well as the removal of residual toluene at TPBs, during the recovery process. This resulted in decreased response, but at the same time, faster recovery. The results demonstrated that both high electrochemical activity of toluene oxidation and low electrochemical activity of oxygen reduction are indispensable for achieving large sensor response. The Au(4CeO<sub>2</sub>)/Pt sensor also showed a nearly linear response vs logarithm of toluene concentration (0.5–50 ppm), with strong response down even to 0.5 ppm toluene (ca. +55 mV) in dry air.

***Keywords: solid-electrolyte gas sensor, YSZ, Au, CeO<sub>2</sub>, toluene***

## 1. Introduction

Volatile organic compounds (VOCs), generated from industrial plants, automobiles, adhesives and paints, are known to contribute to short- and long-term adverse health effects including the so-called *sick building syndrome*, even at relatively low concentrations [1, 2]. For example, Ministry of Health, Labour and Welfare in Japan sets the guideline values for indoor (VOC) concentrations of formaldehyde, toluene, and xylene as 0.08 ppm, 0.07 ppm, and 0.20 ppm, respectively [3]. Therefore, sensitive and selective detection of VOCs is necessary to minimize health risks. However, practical high-performance VOC sensors capable of detecting very low concentration VOC levels are yet to be developed. Among various gas sensors reported so far for this purpose [4–16], solid-electrolyte gas sensors reportedly provide high sensitivity and selectivity when fitted with compositionally and microstructurally optimized sensing electrodes (SE) [8–10, 17–21]. Solid-electrolyte gas sensors utilizing yttria-stabilized zirconia (YSZ) as the solid electrolyte are particularly promising given their exceptional chemical, thermal and mechanical stability [8, 10, 17–22]. Elumalai et al., for example, demonstrated that YSZ-based sensors equipped with a composite Au/NiO SE showed selective response to propylene [23]. Mori et al. reported that YSZ-based sensors equipped with a composite Au/YSZ SE exhibited high sensitivities to low concentrations of methyl mercaptan, hydrogen sulfide, ammonia and trimethylamine [24]. We have focused on composite Au/metal oxide (MO) SEs, given reports that suitable selection of appropriate oxides can promote VOC oxidation [25–27], leading to improved VOC-sensing properties. CeO<sub>2</sub>, in particular, is well known to have a large oxygen-storage capacity and thereby enhances the activities of noble-metal catalysts towards formaldehyde or methane oxidation, given its ability to provide oxygen species in support of oxidation reactions [28, 29]. The doping of Zr<sup>4+</sup> [30, 31] and Pr<sup>4+</sup> [32–34] into CeO<sub>2</sub> further increase its oxygen-storage capacity and thereby its catalytic activity. This follows from the enhanced ability for CeO<sub>2</sub> to become reduced either due to structural relaxations around the smaller Zr<sup>4+</sup> ion, leading to the formation of oxygen vacancies and Ce<sup>3+</sup> or due to the ease of reduction of Pr<sup>4+</sup> to Pr<sup>3+</sup>, even under rather oxidizing

conditions. Pr- and La-doped CeO<sub>2</sub> have also be reported to exhibit relatively high soot-oxidation activity at low temperatures [35]. In addition, the positive effects of the addition of rare-earth oxides such as CeO<sub>2</sub>, La<sub>2</sub>O<sub>3</sub>, Pr<sub>6</sub>O<sub>11</sub>, Nd<sub>2</sub>O<sub>3</sub> and Sm<sub>2</sub>O<sub>3</sub>, to a Pd/SiO<sub>2</sub> catalyst for the CO hydrogenation reaction have also reported [36].

In this study, YSZ-based gas sensors equipped with Au/MO<sub>x</sub> (CeO<sub>2</sub>, Gd<sub>2</sub>O<sub>3</sub>, La<sub>2</sub>O<sub>3</sub>, Pr<sub>6</sub>O<sub>11</sub>, Sm<sub>2</sub>O<sub>3</sub>, Pr<sub>0.1</sub>Ce<sub>0.9</sub>O<sub>2</sub>, Ce<sub>0.8</sub>Zr<sub>0.2</sub>O<sub>2</sub>) composite SEs were fabricated, and their toluene-sensing properties examined. In addition, the impact of the addition of the various metal oxides to the Au-based SEs on the sensing properties are discussed in relation to their effects on the microstructure of the SEs, and the relative catalytic and electrocatalytic activities of the individual Au and MO materials.

## 2. Experimental

### 2.1. Synthesis of MO powder

CeO<sub>2</sub> powder was synthesized by a sol-gel method [37]. After Ce(NO<sub>3</sub>)<sub>3</sub>·6H<sub>2</sub>O was dissolved in dehydrated ethanol, triethanolamine was added to the solution and then stirred for 1 h to form a chelate compound. Subsequently, the obtained compound was hydrolyzed for 1 h by adding a small amount of pure water into the solution. Then, the obtained precipitate was centrifuged and washed with dehydrated ethanol several times. The product was dried at 100°C for 12 h and then annealed at 700°C for 2 h in air. Ce<sub>0.2</sub>Zr<sub>0.8</sub>O<sub>2</sub> (CZO) and Pr<sub>0.1</sub>Ce<sub>0.9</sub>O<sub>2</sub> (PCO) powders were prepared by the Pechini method [33, 37]. Appropriate amounts of citric acid and ethylene glycol were added to an aqueous solution of constituent metal nitrates. The obtained mixture was heated to evaporate volatile species, ultimately forming a dried solid that was ground and calcined at elevated temperature (600°C for 5 h in air for CZO, 700°C for 3 h in air for PCO). The obtained powder was ball milled using zirconia media in alcohol to break up agglomerates. Gd<sub>2</sub>O<sub>3</sub>, La<sub>2</sub>O<sub>3</sub> and Sm<sub>2</sub>O<sub>3</sub> powders were purchased from Kishida Chemical Co., Ltd., Japan. Pr<sub>6</sub>O<sub>11</sub> powder was purchased from Wako Pure Chemical Industries, Ltd., Japan. The specific surface areas of the MO powders were measured by the Brunauer–Emmett–Teller (BET) method using a N<sub>2</sub> adsorption isotherm (Micromeritics Instruments Corp., Tristar3000).

### 2.2. Fabrication of sensors

The schematic structure of a planar-type YSZ-based gas sensor is shown in Fig. 1. Au paste (Tanaka Corp., TR-1403), Au paste mixed with an appropriate amount of MO powder or Au paste mixed with polymethylmethacrylate (PMMA) microspheres (Soken Chem. & Eng. Co., Ltd., MX150, ca. 1500 nm in diameter) was screen printed on the surface of YSZ substrates (Japan Fine Ceramics Co., Ltd, ca. 11 mm in diameter and ca. 0.5 mm in thickness) as a SE (2 mm x 3 mm). This resulted in either dense nominally pure Au electrodes (d-Au), or *n* wt% MO-mixed Au electrode (Au(*n*MO)),

$n = 4, 10, 15$  (wt%) MO) or porous Au electrodes (p-Au), respectively. Pt (Tanaka Corp., TR-7907) paste was also subsequently applied by screen printing on the same surface of the YSZ substrate to serve as the counter electrode (CE, 2 mm x 3 mm). After annealing at 700°C for 2 h in air, planar-type YSZ-based gas sensors (SE/CE sensors, SE: d-Au, p-Au or Au( $n$ MO), CE: Pt), were obtained as shown in Fig. 1. The secondary electron images of the d-Au, p-Au and Au( $n$ MO) SEs were obtained by scanning electron microscopy (SEM; JEOL Ltd., JSM-7500F).

### 2.3. Measurement of toluene-sensing properties

The gas responses of the sensors were examined by measuring the open circuit electromotive force induced across the two sensor electrodes upon exposure to 0.5–50 ppm toluene, balance dry air, under a gas-flow rate of 100 cm<sup>3</sup> min<sup>-1</sup> at temperatures of 400, 450 and 500°C. The electromotive force ( $E$ , mV) of the sensors was measured with a digital electrometer (ADC Corp., 8240). The magnitude of the sensor response ( $\Delta E$ ) was defined as the difference between  $E$  measured upon exposure to toluene and that measured in the base air. The 90% recovery time ( $T_{90\text{rec}}$ ) was defined as the time necessary to reach 90% value of the steady state value of  $\Delta E$ .

### 2.4. Evaluation of catalytic combustion behavior of toluene over sensing materials

Au powder, prepared by drying the Au paste, or MO powders, were pressed into disc, and then crushed into granules (ca. 20–60 mesh). The granules of about 0.6 g, fixed in a glass reactor of the flow apparatus, were exposed to 250 ppm toluene/balance air that was prepared by a gas generator utilizing a diffusion tube (Gastec Corp., PD-1B), at a flow rate of 30 cm<sup>3</sup> min<sup>-1</sup> (a gas hourly space velocity (GHSV) of 5560 h<sup>-1</sup>). The catalytic combustion behavior of the toluene over Au and MO powders was then evaluated in the temperature range from 30 to 300°C, by using a gas chromatograph equipped with FID and TCD detectors (Shimadzu Corp., GC-2010 (capillary column used: DB-5 and PoraPLOT Q, respectively)).

## 2.5 Evaluation of electrochemical activity of toluene

The current ( $I$ )–voltage ( $E$ ) curves of the sensors were measured at a scan rate of  $3 \text{ mV min}^{-1}$  in order to evaluate the magnitude of the anodic reaction of toluene and the cathodic reaction of oxygen at the triple phase boundaries (TPBs). The net toluene-oxidation current was calculated by subtracting the current measured in base air from that in toluene/balance air.

## 3. Results and discussion

**Figure 2** shows SEM images of the surfaces of the YSZ substrate and all of the SEs. The YSZ surface is observed to be relatively dense (Fig. 2(a)) as was the d-Au SE with its surface morphology (micron-sized grains and clear grain boundaries among them) reflecting the YSZ substrate morphology (Fig. 2(b)). The surface of the p-Au SE, on the other hand, was highly porous, resulting from the decomposition of the added PMMA particles (Fig. 2(c)). The Au(4MO) SEs also exhibited porous structures (Fig 2(d-j)), similar to that of the p-Au SE, with the porosity and morphology largely dependent on the specific MOs dispersed within the Au(4MO) SEs. For example, the Au particles in the Au(4Gd<sub>2</sub>O<sub>3</sub>) SE were well interconnected on the surface of the YSZ substrate (Fig. 2(e)). The degree of porosity of the Au(4Gd<sub>2</sub>O<sub>3</sub>) SE was the lowest among the Au(4MO) SEs. The level of porosity in the Au/MO composites increased in the following order: Gd<sub>2</sub>O<sub>3</sub>, CZO, Pr<sub>6</sub>O<sub>11</sub>, Sm<sub>2</sub>O<sub>3</sub>, La<sub>2</sub>O<sub>3</sub>, CeO<sub>2</sub> and PCO.

Figure 3 shows response transients to 50 ppm toluene of all sensors at 500°C in dry air, and Fig. 4 shows the temperature dependence of the magnitude of the response ( $\Delta E$ ) and the recovery time ( $T_{90\text{rec}}$ ) of the d-Au/Pt, p-Au/Pt and Au(4MO)/Pt sensors to 50 ppm toluene. All the sensors responded to toluene with a negative change in  $E$ , with most sensors exhibiting an initial overshoot in  $E$  over the whole operating temperature range as shown in Fig. 3 for the 500°C data. In addition, the magnitude of the toluene response of all sensors increased with decreasing operating temperature.

Among the sensors, the p-Au/Pt and d-Au/Pt sensor showed the largest and smallest responses, respectively, over the whole operating temperature range. Generally, one expects a certain fraction of toluene to be oxidized to CO<sub>2</sub> and H<sub>2</sub>O, as toluene diffuses from the SE surface towards the interface between the SE and the YSZ electrolyte. Thus, an increase in SE porosity enhances gas diffusivity resulting in an increase of toluene reaching the SE/YSZ interface. This likely promotes the electrochemical oxidation of toluene at the Triple Phase Boundaries (TPBs), and thereby enhances the magnitude of the response to toluene. The Au(4MO)/Pt sensors showed a larger response to toluene than the d-Au/Pt sensor, whereas the response of the Au(4MO)/Pt sensors was smaller than that of the p-Au/Pt sensor over the entire operating temperature range. In addition, the toluene response of the Au(4MO)/Pt sensors was strongly influenced by the type of MO mixed into the composite Au/MO SE, with the Au(4CeO<sub>2</sub>)/Pt sensor showing the largest toluene response among all the Au(4MO)/Pt sensors. The Au(4CeO<sub>2</sub>)/Pt, Au(4Gd<sub>2</sub>O<sub>3</sub>)/Pt and Au(4CZO)/Pt sensors showed rather large responses to toluene, while the Au(4Pr<sub>6</sub>O<sub>11</sub>)/Pt and Au(4PCO)/Pt sensors showed smaller responses.

While the comparison of response time of the sensors was somewhat complicated by the overshoot behavior, one clearly observes an inverse dependence of sensor recovery time ( $T_{90\text{rec}}$ ) on operating temperature, as shown in Fig. 4 (b). The  $T_{90\text{rec}}$  value of the p-Au/Pt sensor was the largest, with all the Au(4MO)/Pt sensors showing smaller  $T_{90\text{rec}}$  values than the p-Au/Pt sensor. The Au(4PCO)/Pt sensor showed the smallest  $T_{90\text{rec}}$  value at 400 and 450°C while the Au(4CeO<sub>2</sub>)/Pt sensor showed the smallest at 500°C.

In order to investigate the effects of the MO utilized in the Au/MO composite SEs on the magnitude of the toluene response and its recovery behavior, the relative catalytic conversion efficiency of toluene oxidation over Au or MO powders was examined. Figure 5 shows the temperature dependence of conversion efficiency of 250 ppm toluene over Au and MO powders in dry air. While the oxidation of toluene is observed to begin at 50°C over the Au powder, the

conversion efficiency of toluene was limited to 35%, even at 300°C. On the other hand, the fraction of toluene oxidation over the MO powders was considerably higher than over Au. The temperature at which 50% of toluene was converted,  $T_{50}$ , and the specific surface area (SSA) of the MOs examined are summarized in Table 1. The  $T_{50}$  values of the Ce-based oxides (i.e., CeO<sub>2</sub>, CZO and PCO) were much smaller than those of the other MOs (i.e., Gd<sub>2</sub>O<sub>3</sub>, Pr<sub>6</sub>O<sub>11</sub>, La<sub>2</sub>O<sub>3</sub> and Sm<sub>2</sub>O<sub>3</sub>). Namely, toluene was more effectively oxidized over Ce-based oxides in comparison with the other MOs. One clear factor contributing to the observed higher catalytic activity of the Ce-based oxides, as might be expected, was their larger SSA. In addition, CeO<sub>2</sub> showed larger catalytic activity ( $T_{50}$ : ca. 132°C) than CZO (ca. 167°C) and PCO (ca. 217°C), although the SSA of CeO<sub>2</sub> (ca. 15.1 m<sup>2</sup> g<sup>-1</sup>) was smaller than those of CZO (ca. 26.7 m<sup>2</sup> g<sup>-1</sup>) and PCO (ca. 83.1 m<sup>2</sup> g<sup>-1</sup>). As toluene diffuses from the SE surface to the interface between the SE and the YSZ, a certain amount of toluene is oxidized during transport through the SE and thus the concentration of toluene that arrives at TPBs decreases. Therefore, it is likely that these catalytic activities of toluene oxidation over Au and MO powders have a large influence on the toluene-sensing properties of the sensors. As the addition of MOs into the Au based SEs enhances the reduction in toluene concentration at TPBs due to their high catalytic activity for toluene oxidation, the Au(4MO)/Pt sensors showed smaller toluene response than the p-Au/Pt sensor. In addition, the addition of the MOs into the SE presumably also accelerates the oxidation of the residual toluene at TPBs, following removal of the toluene from the base air. This is likely the source of the decreased  $T_{90\text{rec}}$  values associated with the Au(4MO)/Pt sensors relative to that of the p-Au/Pt sensor.

The toluene response and the recovery time of the Au(4MO)/Pt sensors are not only determined by the catalytic activity of toluene oxidation over the MOs. Figure 6 shows the  $T_{50}$  value dependence of the toluene response ( $\Delta E$ ) and the recovery time ( $T_{90\text{rec}}$ ) of the Au(4MO)/Pt sensors at 400 and 500°C.  $\Delta E$  should increase with an increase in  $T_{50}$ , according to the above discussion, but  $\Delta E$  of the Au(4CeO<sub>2</sub>)/Pt and Au(4CZO)/Pt sensors was much larger than that of the Au(4PCO)/Pt,

Au(4Pr<sub>6</sub>O<sub>11</sub>)/Pt and Au(4Sm<sub>2</sub>O<sub>3</sub>)/Pt sensors, even though the  $T_{50}$  value of CeO<sub>2</sub> and CZO was much smaller than that of PCO, Pr<sub>6</sub>O<sub>11</sub> and Sm<sub>2</sub>O<sub>3</sub>. The  $T_{90rec}$  value tended to increase with increasing  $T_{50}$  value, but several exceptions were found. For example, the  $T_{90rec}$  value of the Au(4PCO)/Pt sensor was smaller than that of the Au(4CeO<sub>2</sub>)/Pt sensor at 400°C, even though the catalytic activity of toluene oxidation over PCO was smaller than that over CeO<sub>2</sub>. One of possible reasons for these apparent discrepancies is the difference in porosity between the Au(4PCO) and the Au(4CeO<sub>2</sub>) SEs (see Fig. 2). Namely, the large porosity of the Au(4PCO)/SE promoted the gas diffusivity from the SE surface to TPBs resulting in smaller  $T_{90rec}$  values for the Au(4PCO)/Pt sensor. However, the  $T_{90rec}$  value of the Au(4CeO<sub>2</sub>)/Pt sensor largely decreased by the increase in the operating temperature to 500°C, and its value was comparable to that of the Au(4PCO)/Pt sensor. This may result from the toluene diffusivity in the Au(4CeO<sub>2</sub>) SE approaching that in the Au(4PCO) SE at 500°C due to the increase in operating temperature. Based on these results, a schematic drawing of the toluene-sensing mechanism of the sensors fabricated in this study can be created and is depicted in Fig. 7. The increase in the porosity of the SEs is considered to increase the actual concentration of toluene reaching TPBs due to enhanced gas diffusivity from the surface of SE to TPBs. This idea confirms the larger  $\Delta E$  of the p-Au/Pt sensor than that of the d-Au/Pt sensor. In addition, the increase in the catalytic activity of toluene oxidation over the SE materials is another important factor. Namely, the toluene concentration at TPBs should be reduced by the increase in the catalytic activity for toluene oxidation during gas diffusion in the SEs. Indeed, the  $\Delta E$ s of the Au(4MO)/Pt sensors were smaller than that of the p-Au/Pt sensor. The increase in the porosity and catalytic activity also decreases the  $T_{90rec}$  value because of the more rapid gas diffusion and the prompt oxidation of residual toluene at TPBs in the recovery process, respectively. However, the  $T_{90rec}$  value of the d-Au/Pt sensor was smaller than that of the p-Au/Pt sensor, although the morphology of the d-Au SE was much denser than that of p-Au SE enough to reduce the gas diffusion. In the case of the d-Au SE, the diffusion rate of toluene inside SE is very slow in comparison with that of oxygen, because the size of toluene

molecule is larger than that of oxygen molecule. This difference might cause the prompt oxidation of residual toluene at TPBs by relatively large amount of oxygen diffused to TPBs, leading to smaller  $T_{90\text{rec}}$  value of the d-Au/Pt sensor.

Interestingly, the Au(4CeO<sub>2</sub>)/Pt sensor showed the largest  $\Delta E$  in spite of it exhibiting the highest catalytic activity of toluene oxidation among all the MOs. Therefore, the electrochemical activity, which proceeds at TPBs of the Au(4MO) SEs, should also be a critical factor determining the  $\Delta E$  and  $T_{90\text{rec}}$  values of the Au(4MO)/Pt sensors. Generally, the VOC-sensing mechanism of solid-electrolyte gas sensors, as discussed in various papers, can be explained on the basis of the mixed potential theory [8–10, 19–20, 22]. The electrochemical oxidation of toluene (Eq. 1) and electrochemical reduction of oxygen (Eq. 2) are expected to simultaneously proceed at the same rate at the SE TPBs in this study.



Figure 8(a) shows the  $I$ - $E$  characteristics of representative sensors (d-Au/Pt, Au(4CeO<sub>2</sub>)/Pt, Au(4Pr<sub>6</sub>O<sub>11</sub>)/Pt) at 500°C in both air and 50 ppm toluene balanced with air. The net anodic current of only toluene oxidation was calculated by subtracting the current in base air from that in toluene/balance air, and the relationship between the net anodic current and the cell potential was plotted in Fig. 8(b), together with the  $I$ - $E$  curves in air. The magnitude of negative current of the d-Au/Pt sensor increased with an increase in the negative potential applied in air, which means that electrochemical reduction of oxygen proceeds at TPBs. The  $I$ - $E$  curve shifted in the positive direction and the open-circuit voltage (OCV) shifted to the negative direction upon exposure to toluene. This indicates that the electrochemical oxidation of toluene proceeds at TPBs in addition to the electrochemical reduction of oxygen. However, the amount of change in OCV was small (ca. -22 mV) and both the net anodic current of the toluene oxidation and the current of the oxygen reduction at OCV in toluene/balance air was small, as shown in Fig. 8(b). In addition, the slope of the  $I$ - $E$

curve of toluene oxidation is much smaller than that of oxygen reduction. As the absolute value of the net anodic current of toluene oxidation should be equal to that of the cathodic current of oxygen reduction in air at OCV in toluene, the d-Au/Pt sensor showed rather small  $\Delta E$  response to toluene. The addition of CeO<sub>2</sub> to the Au SE significantly increased the slope of the  $I-E$  curve positively in both air and toluene/balance air, especially the net anodic current observed increased with an increase in applied potential. This fact means that the electrochemical oxidation of toluene proceeded actively at TPBs in comparison with the electrochemical reduction of oxygen. The modified current of toluene oxidation of the Au(4CeO<sub>2</sub>)/Pt sensor in toluene (ca. 450 nA) was much larger than that of the d-Au/Pt sensor (ca. 13 nA), at ca. -102 mV (OCV in toluene for the Au(4CeO<sub>2</sub>)/Pt sensor). On the other hand, the current of oxygen reduction of the Au(4CeO<sub>2</sub>)/Pt sensor was only 14 times higher than that of the d-Au/Pt sensor, at the same OCV (ca. -102 mV). Therefore, OCV in toluene/balance air of the Au(4CeO<sub>2</sub>)/Pt sensor shifted largely to the negative direction upon exposure to toluene, compared with that of the d-Au/Pt sensor. It was also confirmed that the calculated  $\Delta E$  of the Au(4CeO<sub>2</sub>)/Pt sensor (ca. +102 mV, the difference in OCV in toluene/balance air and that in air) was almost the same value as the observed  $\Delta E$  (ca. +125 mV). The addition of Pr<sub>6</sub>O<sub>11</sub> to the Au SE also increased the slope of the  $I-E$  curve positively as was the case with the Au(4CeO<sub>2</sub>)/Pt sensor as shown in Fig. 8(a). However, the electrochemical activity of the Au(4Pr<sub>6</sub>O<sub>11</sub>)/Pt sensor was different from that of the Au(4CeO<sub>2</sub>)/Pt sensor. The slope of the  $I-E$  curve of the Au(4Pr<sub>6</sub>O<sub>11</sub>)/Pt sensor in air was larger than that of the Au(4CeO<sub>2</sub>)/Pt sensor. On the other hand, the slope of the  $I-E$  curve of the Au(4Pr<sub>6</sub>O<sub>11</sub>)/Pt sensor in toluene/balanced air was comparable to that of the Au(4CeO<sub>2</sub>)/Pt sensor. In addition, the large net anodic current for toluene oxidation was almost independent of the applied potential values. Therefore, OCV in toluene balanced with air of the Au(4Pr<sub>6</sub>O<sub>11</sub>)/Pt sensor also shifted to the negative direction upon exposure to toluene, but the amount of the change in OCV was smaller than that of the Au(4CeO<sub>2</sub>)/Pt sensor. However, the net anodic current for toluene oxidation and the cathodic current for oxygen oxidation of the Au(4Pr<sub>6</sub>O<sub>11</sub>)/Pt sensor at OCV in toluene were

larger than those of the Au(4CeO<sub>2</sub>)/Pt sensor. Namely, the addition of Pr<sub>6</sub>O<sub>11</sub> enhanced the electrocatalytic activities, but the increment of oxygen reduction is much larger than that of toluene oxidation, which resulted in the smaller change in OCV of the Au(4Pr<sub>6</sub>O<sub>11</sub>)/Pt sensor than that of the Au(4CeO<sub>2</sub>)/Pt sensor. Therefore, the electrochemical activity at TPBs can significantly influence the change in  $\Delta E$  on the basis of the mixed potential theory [8-10, 19–20, 22], and both the increase in toluene oxidation and the decrease in oxygen reduction affects the increment of  $\Delta E$ , as shown in Fig. 7. In addition, high electrochemical activity should also decrease the  $T_{90\text{rec}}$  value, because the toluene is quickly removed at TPBs. However, this issue requires further clarification.

Figure 9 shows the variations in  $\Delta E$  and  $T_{90\text{rec}}$  at 400°C of the Au( $n$ CeO<sub>2</sub>)/Pt and Au( $n$ CZO)/Pt sensors to 50 ppm toluene as a function of the wt% MO ( $n$ ) mixed into the Au SE.  $\Delta E$  of both sensors decreased with increase in  $n$ , and  $\Delta E$  of the Au( $n$ CeO<sub>2</sub>)/Pt sensor was more strongly dependent on  $n$ , in comparison with that of the Au( $n$ CZO)/Pt sensor. This is likely related to the larger catalytic activity of toluene oxidation over CeO<sub>2</sub> that reduced the actual concentration of toluene at TPBs due to the effective oxidation of toluene in the SE. However, the level of porosity of the SE also influences the response. Figure 10 shows SEM images of the surface structure of the Au( $n$ CeO<sub>2</sub>) and Au( $n$ CZO) SEs ( $n = 10$  and  $15$ ), that should be compared with those of the Au(4CeO<sub>2</sub>) and Au(4CZO) SEs (Fig. 2(d) and Fig. 2(i), respectively). These images showed that the porosity of the Au( $n$ CeO<sub>2</sub>) and Au( $n$ CZO) SEs increased with wt% CeO<sub>2</sub> and CZO. In addition, the Au( $n$ CeO<sub>2</sub>) SE showed a more porous structure than that of the Au( $n$ CZO) SE. These results indicate the impact of catalytic activity on the decrease in  $\Delta E$  is greater than that of gas diffusivity. In addition, the  $T_{90\text{rec}}$  value of both sensors decreased with increased wt% MO, and the Au( $n$ CeO<sub>2</sub>)/Pt sensors showed smaller  $T_{90\text{rec}}$  values than that of the Au( $n$ CZO)/Pt sensors. As the catalytic activity and the magnitude of porosity of the SEs of the Au( $n$ CeO<sub>2</sub>)/Pt sensors is higher than that of the Au( $n$ CZO)/Pt sensors, the decrease in the  $T_{90\text{rec}}$  value probably arises from the effective oxidation and gas diffusion of the residual toluene at TPBs following removal of toluene from the base air.

Figure 11 shows toluene-concentration dependences of  $\Delta E$  and response transients to 0.5 ppm toluene of the Au(4CeO<sub>2</sub>)/Pt sensor at 400, 450 and 500°C in dry air. The sensor showed an almost linear relationship between the  $\Delta E$  and the logarithm of toluene concentration over the whole operating temperature range. In addition, the slope, i.e., toluene sensitivity, increased with a decrease in the operating temperature, and the sensor showed the largest sensitivity at 400°C (ca. 75 mV/decade). The Au(4CeO<sub>2</sub>)/Pt sensor showed a large response even to 0.5 ppm toluene (ca. +55 mV) with relatively slow response and recovery speeds at 400°C, while the rise in operating temperature reduced the magnitude of the response (ca. +19 mV at 500°C) but accelerated the response and recovery speeds. These results demonstrate the ability of the optimized Au(4CeO<sub>2</sub>)/Pt sensor to readily detect low concentrations of toluene with high sensitivity, particularly at the lower operating temperatures.

#### 4. Conclusions

The toluene-sensing properties of d-Au/Pt, p-Au/Pt and Au(4MO)/Pt sensors were examined and the effects of MO additions to the Au electrode on the toluene-sensing properties discussed. Au(4MO)/Pt sensors showed larger response to toluene than the d-Au/Pt sensor, with the Au(4CeO<sub>2</sub>)/Pt sensor showing the largest  $\Delta E$  among all of the Au(4MO)/Pt sensors. However, the  $\Delta E$  of the Au(4CeO<sub>2</sub>)/Pt sensor was smaller than that of the p-Au/Pt sensor, while the  $T_{90\text{rec}}$  value of the Au(4CeO<sub>2</sub>)/Pt sensor was much smaller than that of the p-Au/Pt sensor. The catalytic activity of toluene oxidation over CeO<sub>2</sub> was the largest among all of the powders tested. This high catalytic activity enhanced the amount of toluene oxidized during its diffusion in the Au(4CeO<sub>2</sub>) SE and the removal of residual toluene at TPBs in the recovery process, resulting in the decrease in  $\Delta E$  and the  $T_{90\text{rec}}$  values respectively. The addition of CeO<sub>2</sub> to the Au SE also enhanced its electrochemical activity, especially with respect to toluene oxidation. On the other hand, the addition of Pr<sub>6</sub>O<sub>11</sub> to the Au SE preferentially promoted oxygen reduction as well as toluene oxidation, resulting in smaller

$\Delta E$  than that of the Au( $4\text{CeO}_2$ )/Pt sensor. These results indicate that both the high electrochemical activity of toluene oxidation and the low electrochemical activity of oxygen reduction are indispensable for achieving large  $\Delta E$ . The Au( $4\text{CeO}_2$ )/Pt sensor also showed a nearly linear relationship between  $\Delta E$  and the logarithm of toluene concentration (0.5–50 ppm) with large response even down to 0.5 ppm toluene (ca. +55 mV) in dry air.

***Acknowledgements:*** Work at Nagasaki University was supported by JSPS KAKENHI Grant Number JP16K18239. Work at MIT was supported by the U.S. Department of Energy (DOE), Office of Science, Basic Energy Sciences (BES) under Award # DE-SC0002633.

## References

1. L. Molhave, G. Clausen, B. Berglund, J. D. Ceaurriz, A. Kettrup, T. Lindvall, M. Maroni, A. C. Pickering, U. Risse, H. Rothweiler, B. Seifert and M. Younes, Total volatile organic compounds (TVOC) in Indoor air quality investigations, *Indoor Air*, 7 (1997) 225–240.
2. Y. Gong, Y. Wei, J. Cheng, T. Jiang, L. Chen, B. Xu, Health risk assessment and personal exposure to Volatile Organic Compounds (VOCs) in metro carriages — A case study in Shanghai, China, *Sci. Total Environ.*, 754 (2017) 1432–1438.
3. Committee on Sick House Syndrome: Indoor Air Pollution Progress Report No. 4, [www.nihs.go.jp/mhlw/chemical/situnai/kentoukai/repeng4.html](http://www.nihs.go.jp/mhlw/chemical/situnai/kentoukai/repeng4.html), 2002, (accessed 14.05.17).
4. M. Mori, Y. Itagaki, J. Iseda, Y. Sadaoka, T. Ueda, H. Mitsuhashi, M. Nakatani, Influence of VOC structures on sensing property of SmFeO<sub>3</sub> semiconductive gas sensor, *Sens. Actuators B* 202 (2014) 873–877.
5. X. Yang, V. Sallesa, Y. V. Kaneti, M. Liu, M. Maillard, C. Journeta, X. Jiang, A. Brioude, Fabrication of highly sensitive gas sensor based on Au functionalized WO<sub>3</sub> composite nanofibers by electrospinning, *Sens. Actuators B* 220 (2015) 1112–1119.
6. M.-H. Seo, M. Yuasa, T. Kida, J.-S. Huh, N. Yamazoe, K. Shimanoe, Microstructure control of TiO<sub>2</sub> nanotubular films for improved VOC sensing, *Sens. Actuators B* 154 (2011) 251–256.
7. K. Kanda, T. Maekawa, Development of a WO<sub>3</sub> thick-film-based sensor for the detection of VOC, *Sens. Actuators B* 108 (2005) 97–101.
8. T. Sato, V. Plashnitsa, M. Utiyama, N. Miura, Potentiometric YSZ-based sensor using NiO sensing electrode aiming at detection of volatile organic compounds (VOCs) in air environment, *Electrochem. Commun.* 12 (2010) 524–526.
9. T. Kida, N. Morinaga, S. Kishi, K. An, K. Sim, B. Chae, J. Kim, B. Ryu, K. Shimanoe, Electrochemical detection of volatile organic compounds using a Na<sub>3</sub>Zr<sub>2</sub>Si<sub>2</sub>PO<sub>12</sub>/Bi<sub>2</sub>Cu<sub>0.1</sub>V<sub>0.9</sub>O<sub>5.35</sub> heterojunction device, *Electrochim. Acta* 56 (2011) 7484–7490.
10. Y. Fujio, V. V. Plashnits, P. Elumalai, N. Miura, Stabilization of sensing performance for mixed-potential-type zirconia-based hydrocarbon sensor, *Talanta* 85 (2011) 575–581.
11. M.A. Ryan, A.V. Shevade, H. Zhou, M. L. Homer, Polymer-carbon black composite sensors in an electronic nose for air-quality monitoring. *MRS Bull.* 29 (2004) 714–719.
12. H. Yuan, B.-H. Kang, H.-M. Jeong, H.-C. Kwon, S.-H. Yeom, J.-S. Lee, D.-H. Kwon, S.-W. Kang, Room temperature VOC gas detection using a gated lateral BJT with an assembled solvatochromic dye, *Sens. Actuators B* 187 (2013) 288–294.
13. Y. Paska, T. Stelzner, S. Christiansen, H. Haick, Enhanced sensing of non polar volatile organic compounds by silicon nanowire field effect transistors, *ACS Nano* 5 (2011) 5620–5626.
14. X. Ning, C. Zhao, F. Shi, S. Jin, Multipoint chemical vapor measurement by zeolite thin film-coated Fresnel reflection-based fiber sensors with an array-waveguide grating, *Sens. Actuators B* 227 (2016) 533–538.

15. Md. R. R. Khan and S.-W. Kang, A high sensitivity and wide dynamic range fiber-optic sensor for low-concentration VOC gas detection, *Sensors* 14 (2014) 23321–23336.
16. R. Das, S. Biswas, R. Bandyopadhyay, P. Pramanik, Polymerized linseed oil coated quartz crystal microbalance for the detection of volatile organic vapours, *Sens. Actuators B* 185 (2013) 293–300.
17. S. Thiemann, R. Hartung, U. Guth, U. Schönauer, Chemical modifications of Au-electrodes on YSZ and their Influence on the non-Nernstian behaviour, *Ionics* 2(5) (1996) 463–467.
18. R. Mukundan, E. L. Brosha, D. R. Brown, F. H. Garzon, Ceria-electrolyte-based mixed potential sensors for the detection of hydrocarbons and carbon monoxide, *Electrochem. Solid State Lett.* 2(8) (1999) 412–414.
19. J. Zosel, D. Westphal, S. Jakobs, R. Müller, U. Guth, Au-oxide composites as HC-sensitive electrode material for mixed potential gas sensors, *Solid State Ion.* 152-153 (2002) 525–529.
20. E. L. Brosha, R. Mukundan, D. R. Brown, F. H. Garzon, Mixed potential sensors using lanthanum manganate and terbium yttrium zirconium oxide electrodes, *Sens. Actuators B* 87(1) (2002) 47–57.
21. P. S. Zhang, U. Guth, A planar thick film sensor for hydrocarbon monitoring in exhaust gases, *Sens Actuators B* 99 (2004) 258–263.
22. N. Miura, T. Sato, S. A. Anggraini, H. Ikeda, S. Zhuiykov., A review of mixed-potential type zirconia-based gas sensors, *Ionics* 20 (2014) 901–925.
23. P. Elumalai, V. V. Plashnitsaa, Y. Fujio N. Miura, Highly sensitive and selective stabilized zirconia-based mixed-potential-type propene sensor using NiO/Au composite sensing-electrode, *Sens. Actuators B* 144 (2010) 215–219.
24. M. Mori, Y. Itagaki, Y. Sadaoka, S. Nakagawa, M. Kida, T. Kojima, Detection of offensive odorant in air with a planar-type potentiometric gas sensor based on YSZ with Au and Pt electrodes, *Sens. Actuators B* 191 (2014) 351–355.
25. S.A.C. Carabineiro, X. Chen, O. Martynyuk, N. Bogdanchikova, M. Avalos-Borja, A. Pestryakov, P.B. Tavares, J.J.M. Órfão, M.F.R. Pereira, J.L. Figueiredo, Gold supported on metal oxides for volatile organic compounds total oxidation, *Catal. Today*, 244 (2015) 103–114.
26. Y. Liu, H. Dai, J. Deng, S. Xie, H. Yang, W. Tan, W. Han, Y. Jiang, G. Guo, Mesoporous Co<sub>3</sub>O<sub>4</sub>-supported gold nanocatalysts: Highly active for the oxidation of carbon monoxide, benzene, toluene, and oxylene, *J. Catal.* 309 (2014) 408–418.
27. Q. Ye, J. Zhao, F. Huo, D. Wang, S. Cheng, T. Kang, H. Dai, Nanosized Au supported on three-dimensionally ordered mesoporous  $\beta$ -MnO<sub>2</sub>: Highly active catalysts for the low-temperature oxidation of carbon monoxide, benzene, and toluene, *Microporous Mesoporous Mat.* 172 (2009) 20–29.
28. Y. Gu, C. Liu, Y. Li, X. Sui, K. Wang, Z. Wang, Ce<sub>0.8</sub>Sn<sub>0.2</sub>O<sub>2</sub>-C composite as a co-catalytic support for Pt catalysts toward methanol electro oxidation, *J. Power Sources* 265 (2014) 335–344.

29. J. Zhang, Y. Jin, C. Li, Y. Shen, L. Han, Z. Hu, X. Di, Z. Liu, Creation of three-dimensionally ordered macroporous Au/CeO<sub>2</sub> catalysts with controlled pore sizes and their enhanced catalytic performance for formaldehyde oxidation, *Appl. Catal. B- Environ.* 91 (2009) 11–20.
30. A. Uzunoglu, H. Zhang, S. Andreescu, L. A. Stanciu, CeO<sub>2</sub>–MO<sub>x</sub> (M: Zr, Ti, Cu) mixed metal oxides with enhanced oxygen storage capacity, *J. Mater. Sci.* 50 (2015) 3750–3762.
31. R. D. Monte, J. Kas̆par, Heterogeneous environmental catalysis – a gentle art: CeO<sub>2</sub>–ZrO<sub>2</sub> mixed oxides as a case history, *Catal. Today* 100 (2005) 27–35.
32. S. R. Bishop, T. S. Stefanik, H. L. Tuller, Defects and transport in Pr<sub>x</sub>Ce<sub>1-x</sub>O<sub>2-δ</sub>: composition trends, *J. Mater. Res.* (2012) 2009–2016.
33. S. R. Bishop, T. S. Stefanikw, H. L. Tuller, Electrical conductivity and defect equilibria of Pr<sub>0.1</sub>Ce<sub>0.9</sub>O<sub>2-δ</sub>, *Phys. Chem. Chem. Phys.* 13 (2011) 10165–10173.
34. Z. Song, W. Liu, H. Nishiguchi, A. Takami, K. Nagaoka, Y. Takita, The Pr promotion effect on oxygen storage capacity of Ce–Pr oxides studied using a TAP reactor, *Appl. Catal. A- Gen.* 329 (2007) 86–92.
35. K. Harada, T. Oishi, S. Hamamoto, T. Ishihara, Lattice oxygen activity in Pr- and La-doped CeO<sub>2</sub> for low-temperature soot oxidation, *J. Phys. Chem. C* 118 (2014) 559–568.
36. J. S. Eieck, A. T. Bell, Studies of the Interactions of H<sub>2</sub> and CO with Pd/SiO<sub>2</sub> Promoted with La<sub>2</sub>O<sub>3</sub>, CeO<sub>2</sub>, Pr<sub>6</sub>O<sub>11</sub>, Nd<sub>2</sub>O<sub>3</sub>, and Sm<sub>2</sub>O<sub>3</sub>, *J. Catal.*, **99** (1986) 278-292.
37. M. Kuhn, S.R. Bishop, J.L.M. Rupp, H.L. Tuller, Structural characterization and oxygen nonstoichiometry of ceria-zirconia (Ce<sub>1-x</sub>Zr<sub>x</sub>O<sub>2-δ</sub>) solid solutions, *Acta Mater.* 61 (2013) 427–4288.

### Figure captions

- Fig.1. Schematic view of a YSZ-based gas sensor.
- Fig.2. SEM photographs of the surface structure of the YSZ substrate and the SEs of the d-Au/Pt, p-Au/Pt and Au(4MO)/Pt sensors.
- Fig.3. Response transients to 50 ppm toluene of the d-Au/Pt, p-Au/Pt and Au(4MO)/Pt sensors at 500°C
- Fig.4. (a) Temperature dependence of 50 ppm toluene response ( $\Delta E$ ), and (b) temperature dependence of 90% recovery time ( $T_{90\text{rec}}$ ) of the d-Au/Pt, p-Au/Pt and Au(4MO)/Pt sensors.
- Fig.5. Temperature dependence of conversion of 250 ppm toluene over Au and MO powders in air.
- Fig.6. (a)  $T_{50}$  dependence of 50 ppm toluene response ( $\Delta E$ ), and (b)  $T_{50}$  dependence of 90% recovery time ( $T_{90\text{rec}}$ ) of the Au(4MO)/Pt sensors.
- Fig.7. Schematic view of the elements for improving the sensing properties.
- Fig.8. (a) Actual and (b) modified current-voltage characteristics of (i) d-Au/Pt, (ii) Au(4CeO<sub>2</sub>)/Pt and Au(4Pr<sub>6</sub>O<sub>11</sub>)/Pt sensors in the potential range of -200 to 0 mV (vs. Pt-CE) in base air and 50 ppm toluene balanced with air.
- Fig.9. (a) Variations in  $\Delta E$ , and (b) variations in  $T_{90\text{rec}}$  to the mixing amount of MO<sub>x</sub> of the Au(*n*MO)/Pt sensors at 400°C (*n*: 4, 10, 15).
- Fig.10. SEM photographs of the surface structure of SEs of the Au(*n*CeO<sub>2</sub>)/Pt and Au(*n*CZO)/Pt sensors (*n*: 10, 15).
- Fig.11. (a) Concentration dependence of toluene response, and (b) response transient to 0.5 ppm toluene of the Au(4CeO<sub>2</sub>)/Pt sensor at 400, 450, 500°C.

Table 1 Temperature at which 50% of toluene was converted ( $T_{50}$ ) and the specific surface area (SSA) of the MO powders.

Table 1. Ueda et al.

Sample	CeO <sub>2</sub>	Gd <sub>2</sub> O <sub>3</sub>	La <sub>2</sub> O <sub>3</sub>	Pr <sub>6</sub> O <sub>11</sub>	Sm <sub>2</sub> O <sub>3</sub>	CZO	PCO
$T_{50} / ^\circ\text{C}$	132	266	266	267	281	167	217
$S / \text{m}^2 \text{g}^{-1}$	15.1	5.3	3.6	2.1	2.2	26.7	83.1

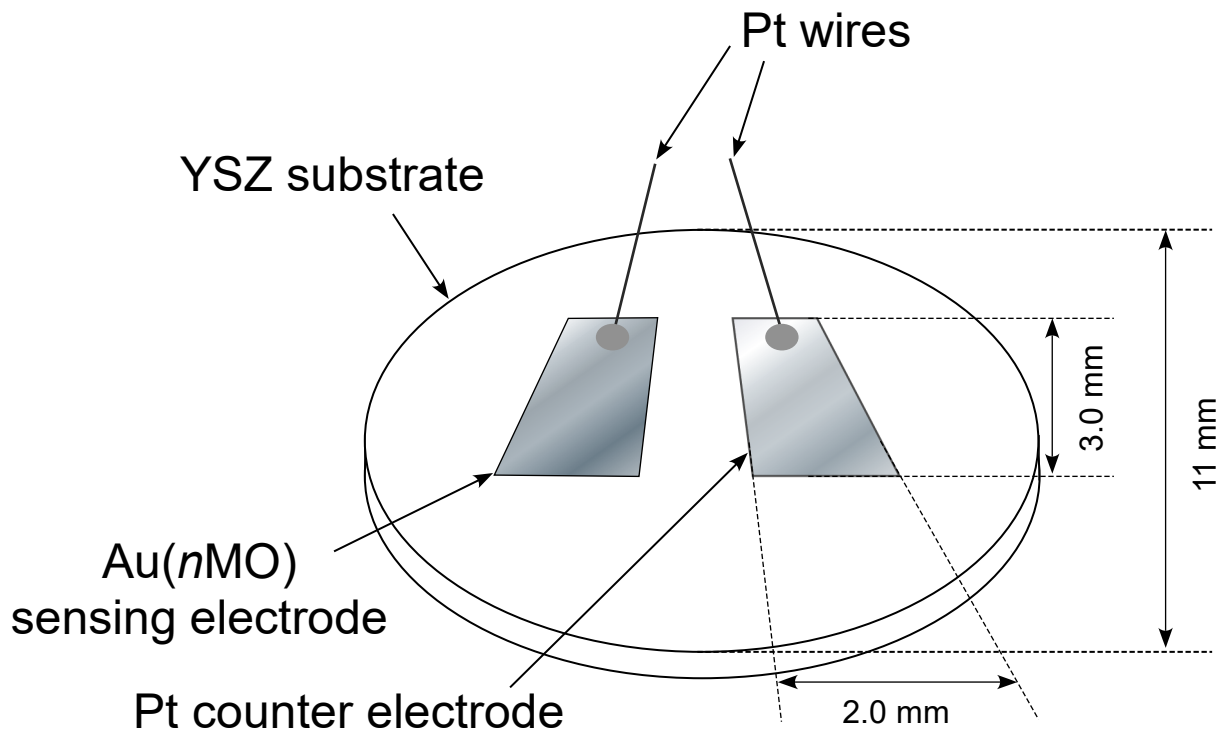


Fig. 1. Ueda et al.

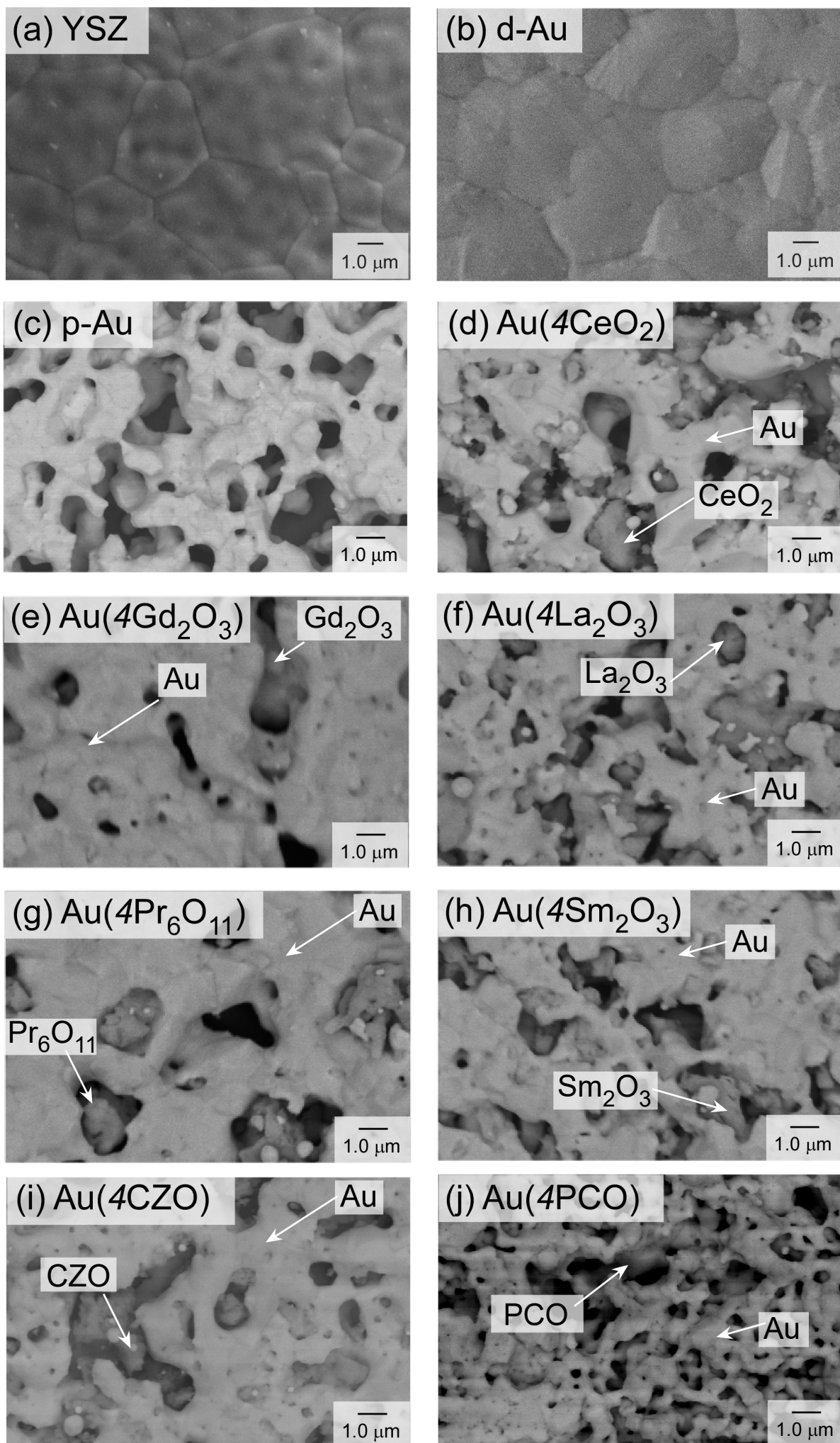


Fig. 2. Ueda et al.

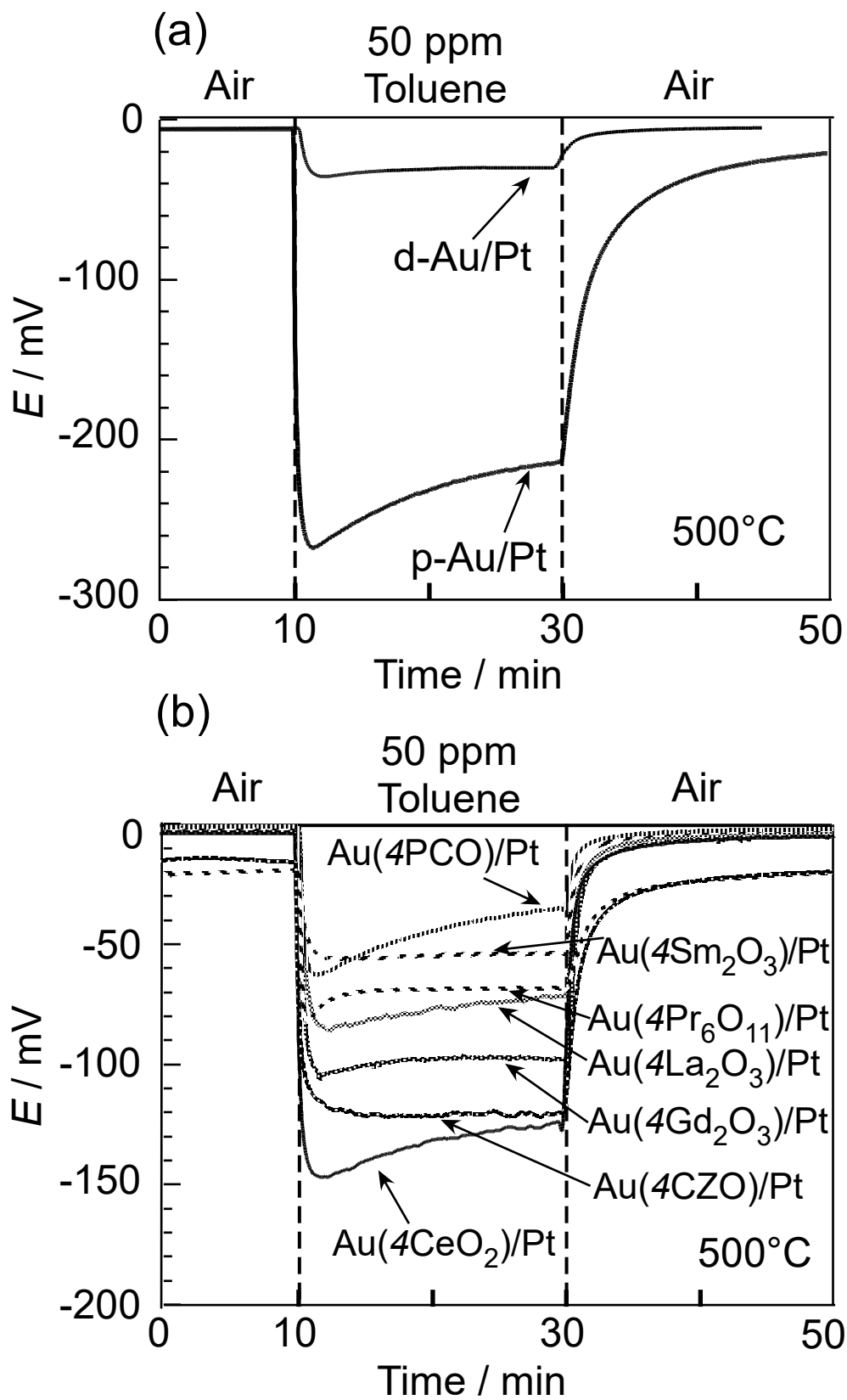


Fig. 3. Ueda et al.

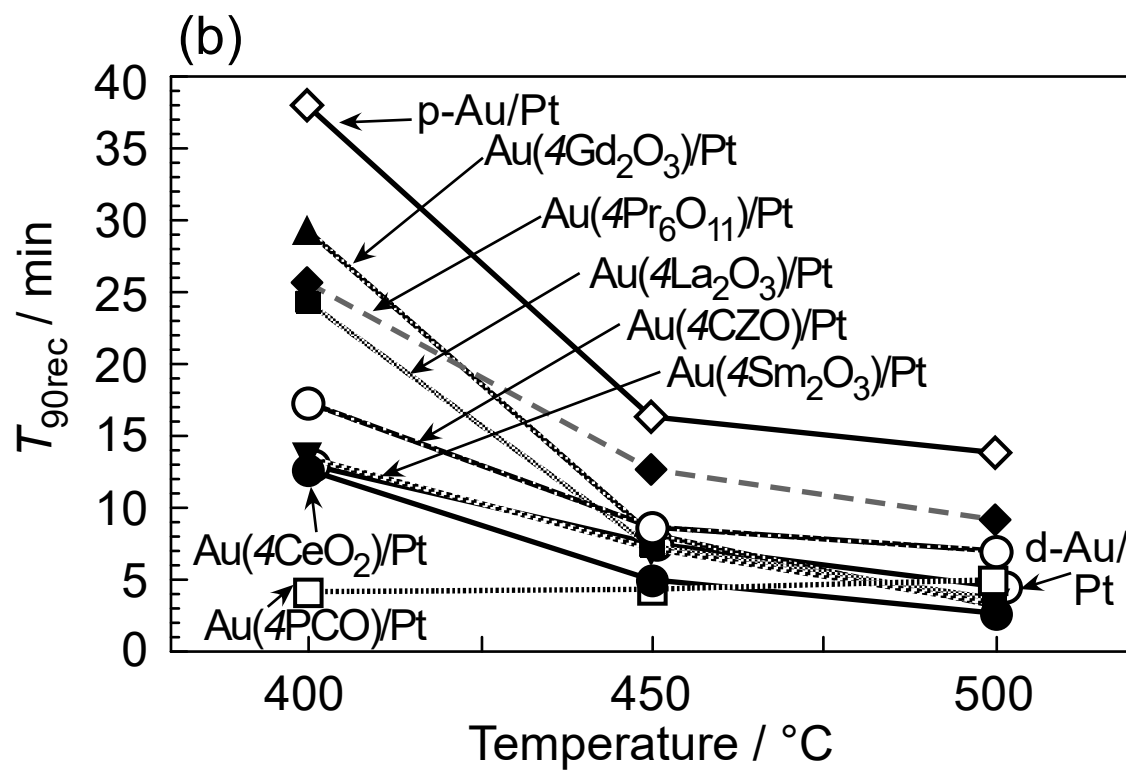
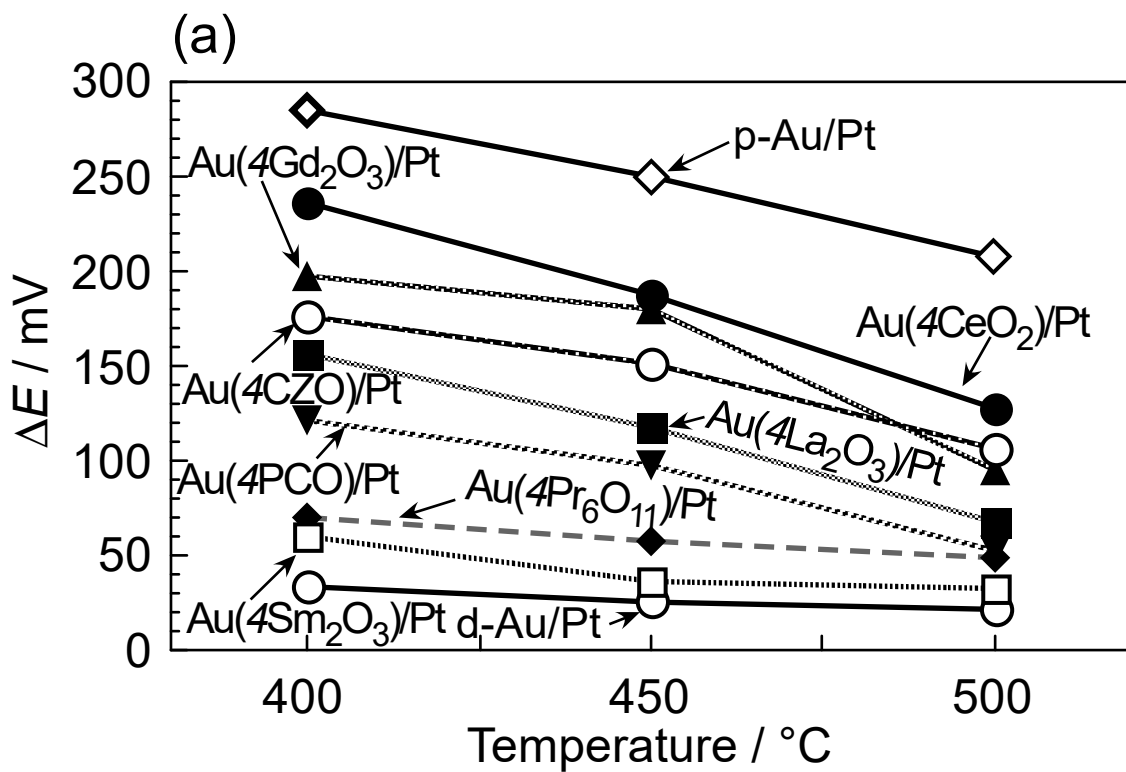


Fig. 4. Ueda et al.

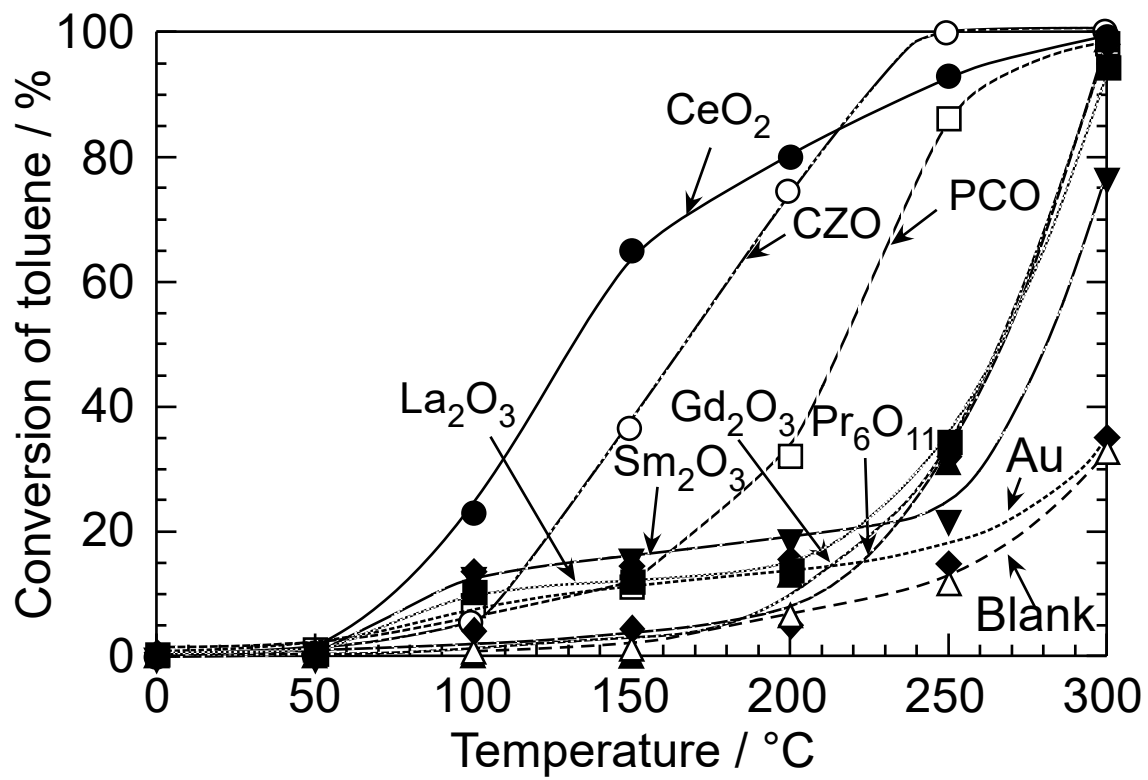


Fig. 5. Ueda et al.

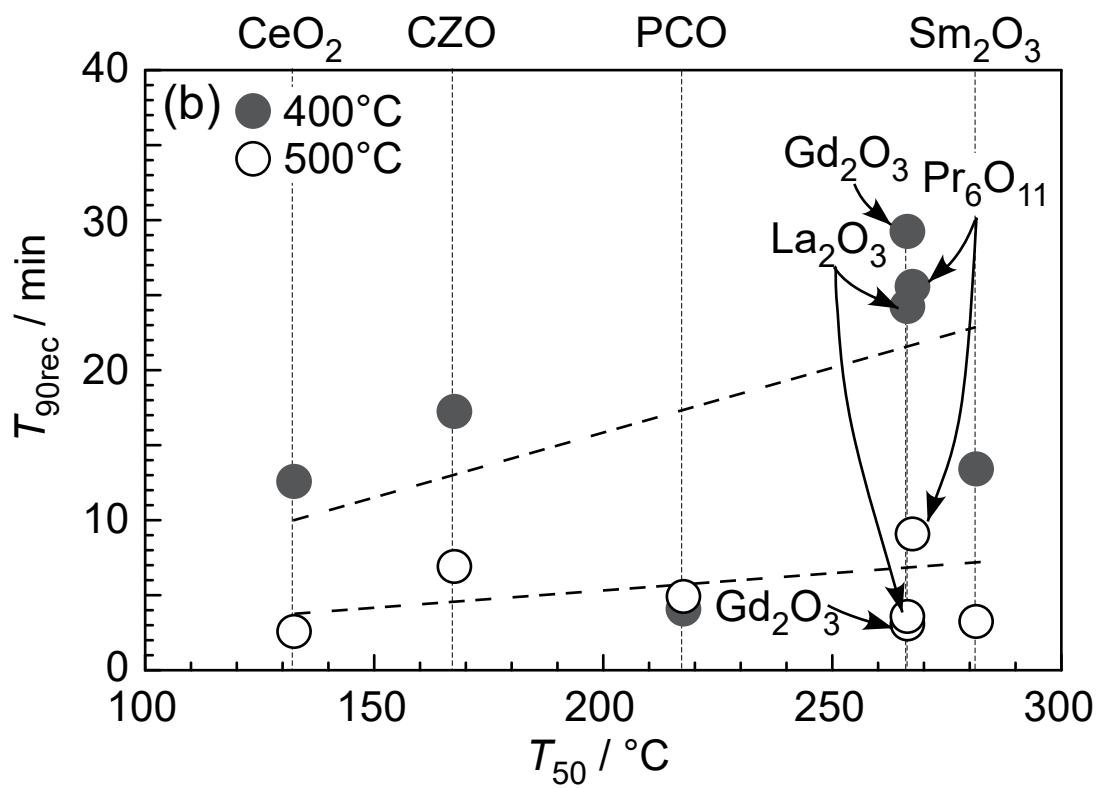
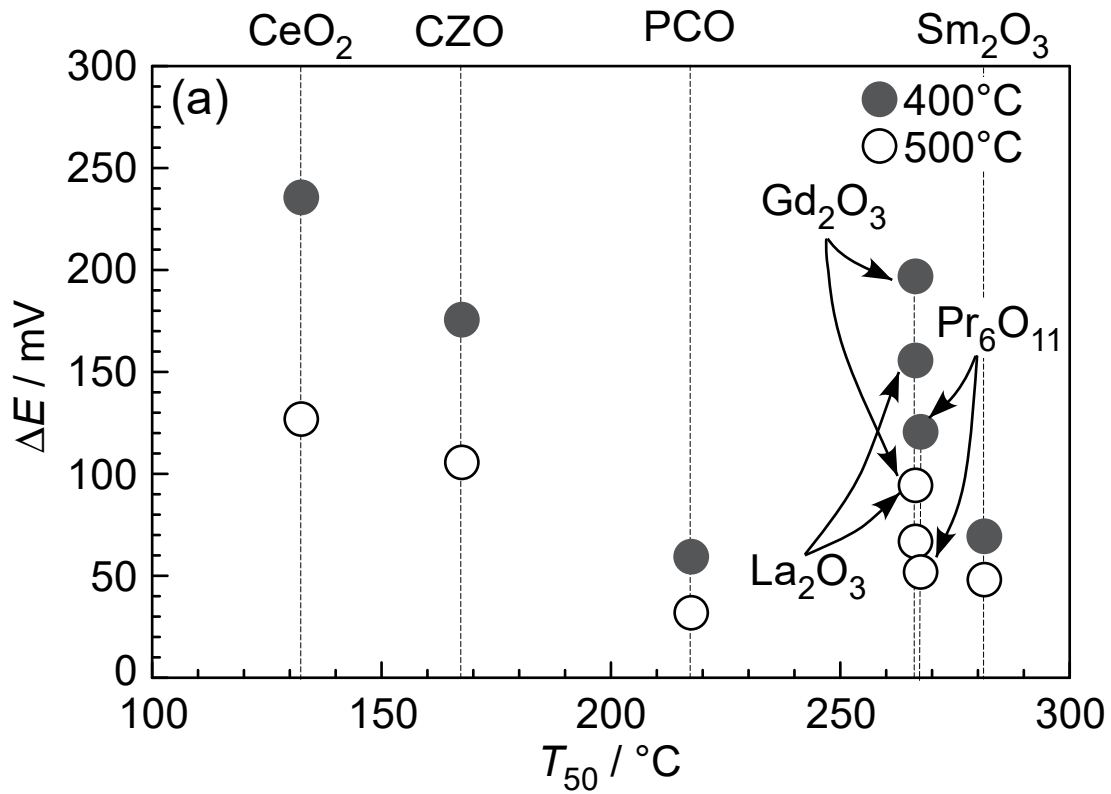


Fig. 6. Ueda et al.

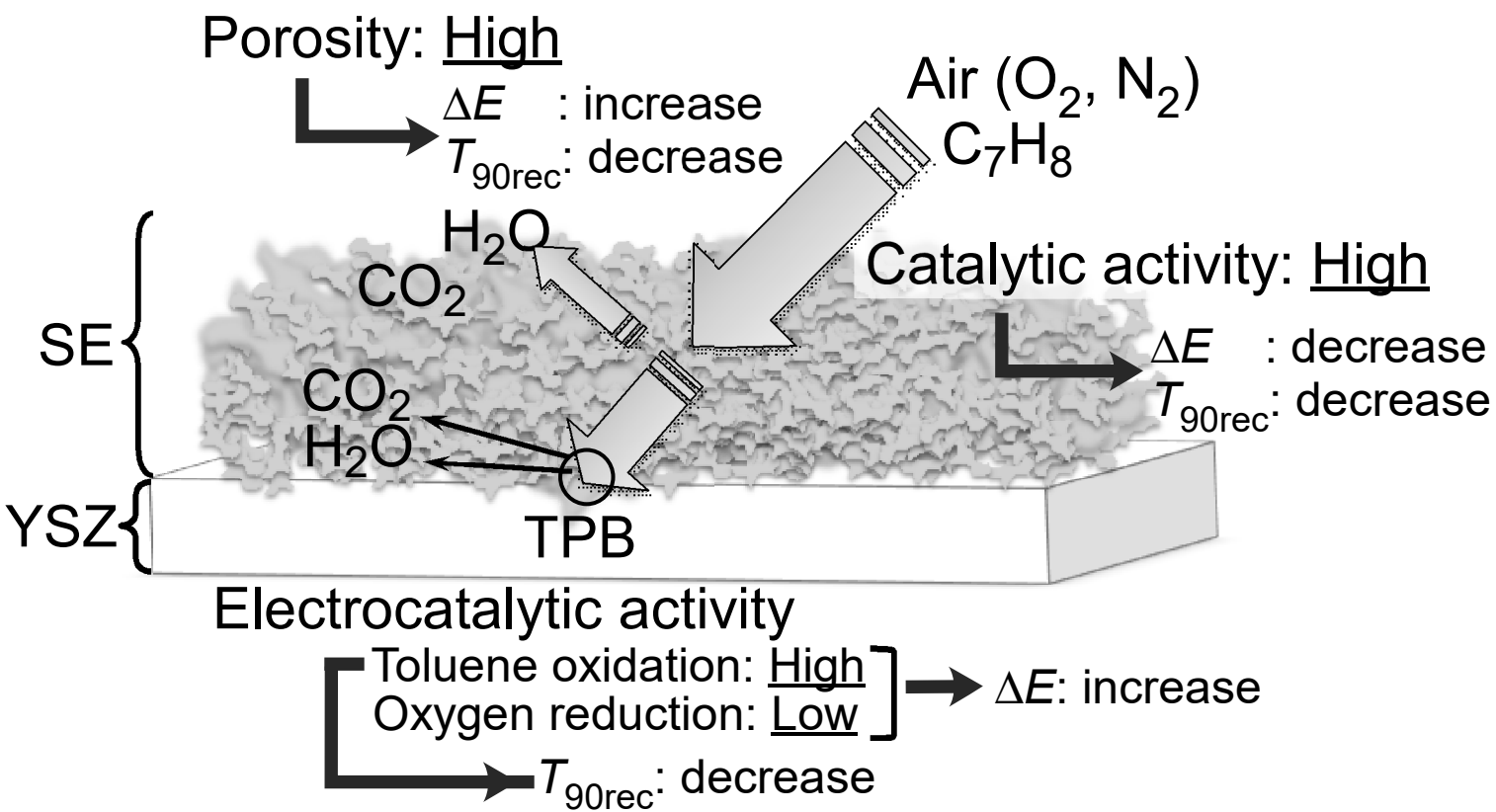


Fig. 7. Ueda et al.

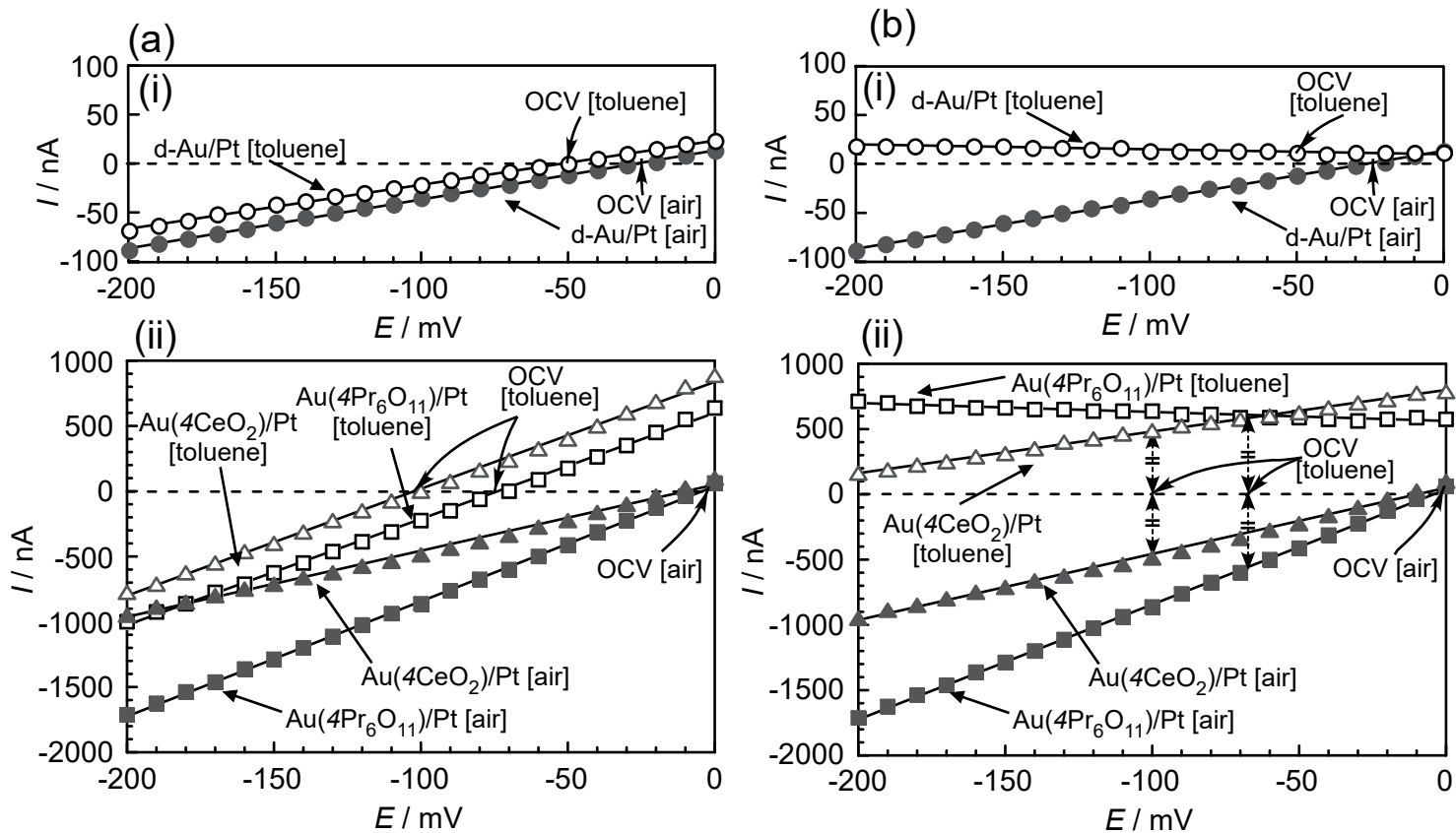
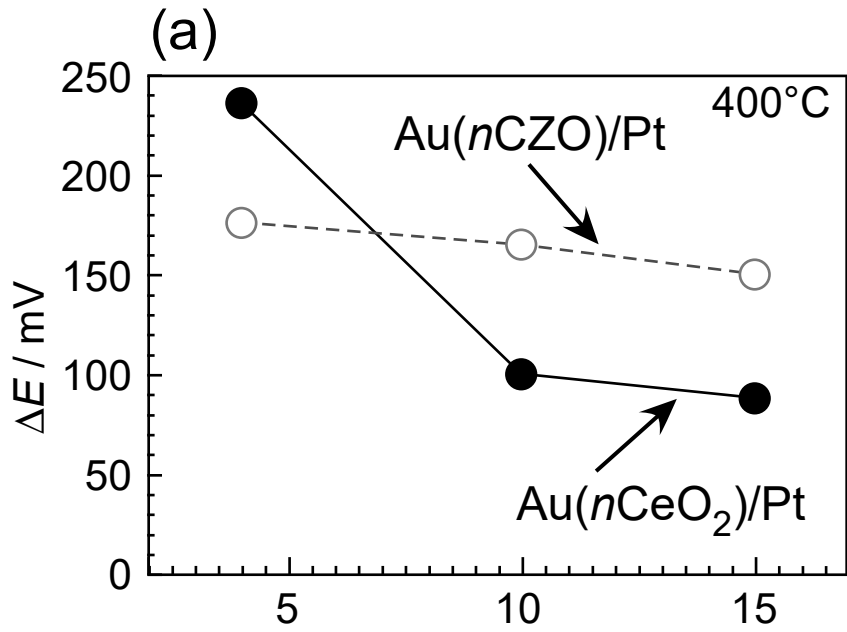
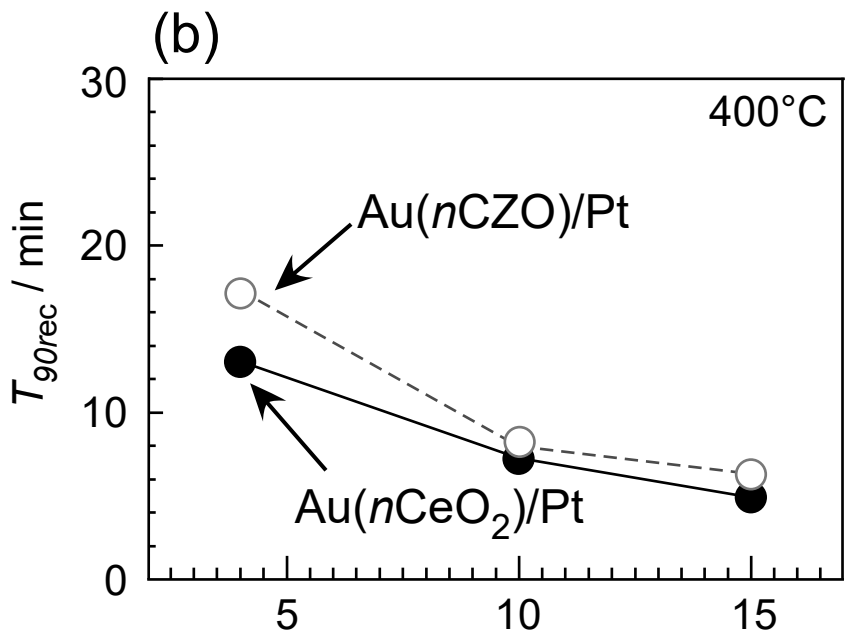


Fig. 8. Ueda et al.



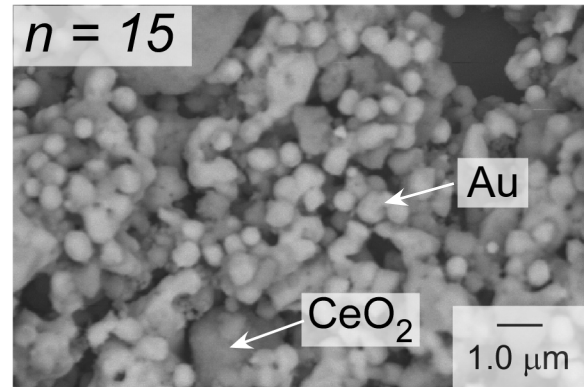
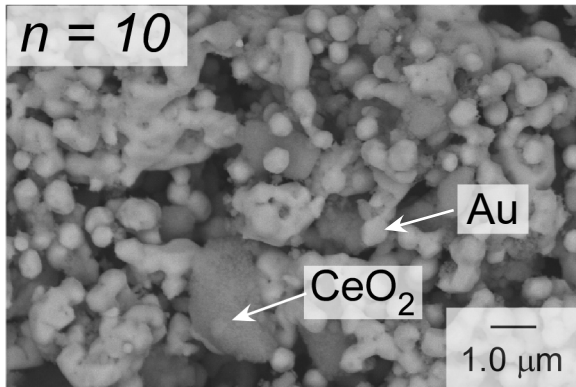
The amounts of MO added into the Au SE ( $n$ ) / wt%



The amounts of MO added into the Au SE ( $n$ ) / wt%

Fig. 9. Ueda et al.

(a)  $\text{Au}(n\text{CeO}_2)$



(b)  $\text{Au}(n\text{CZO})$

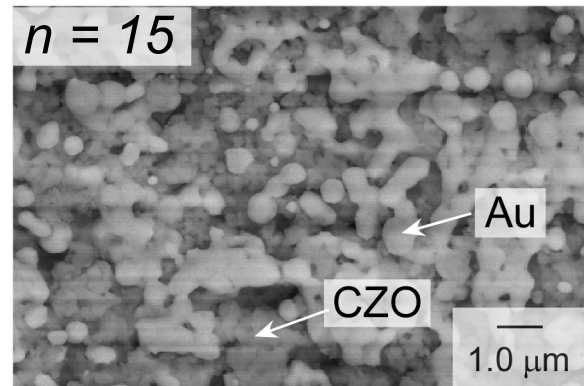
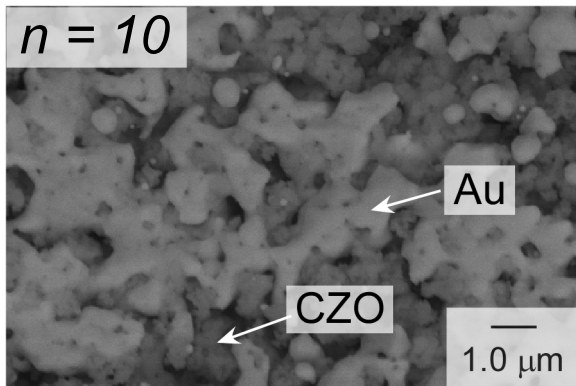


Fig. 10. Ueda et al.

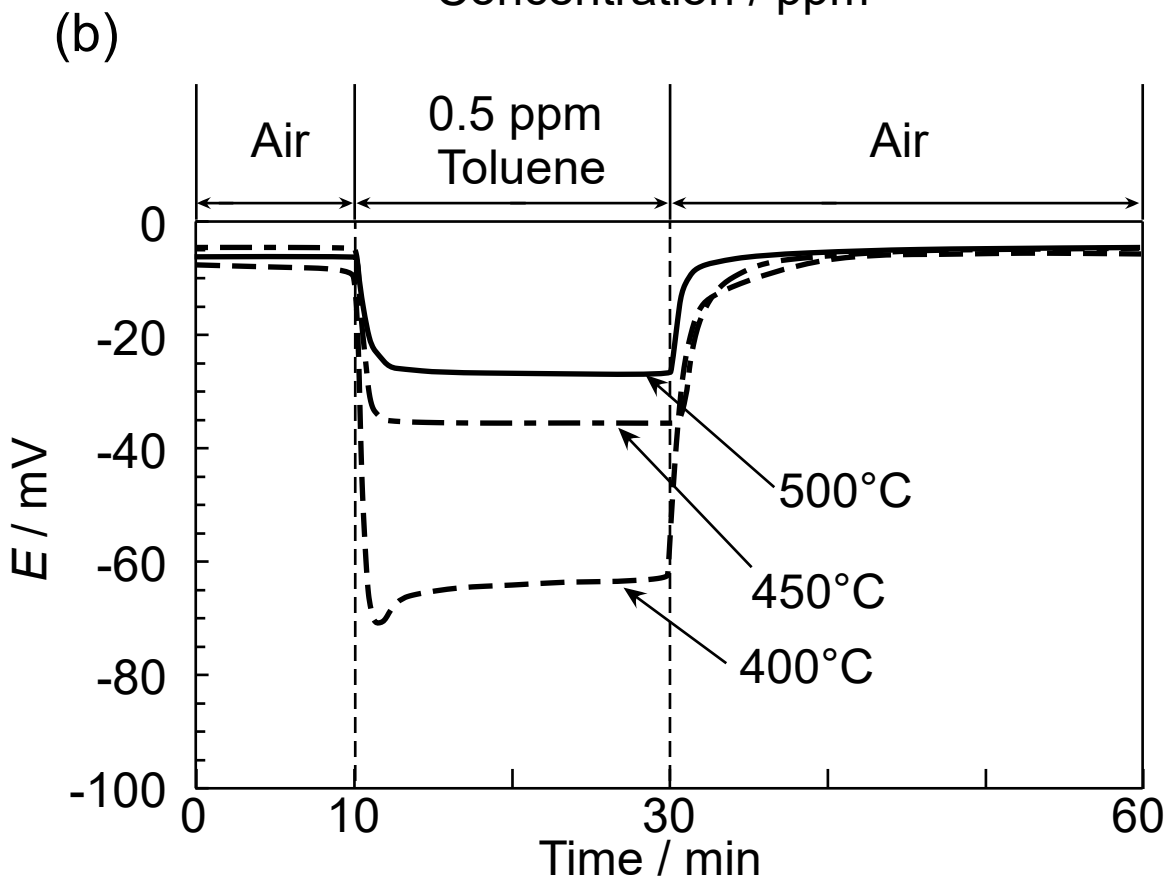
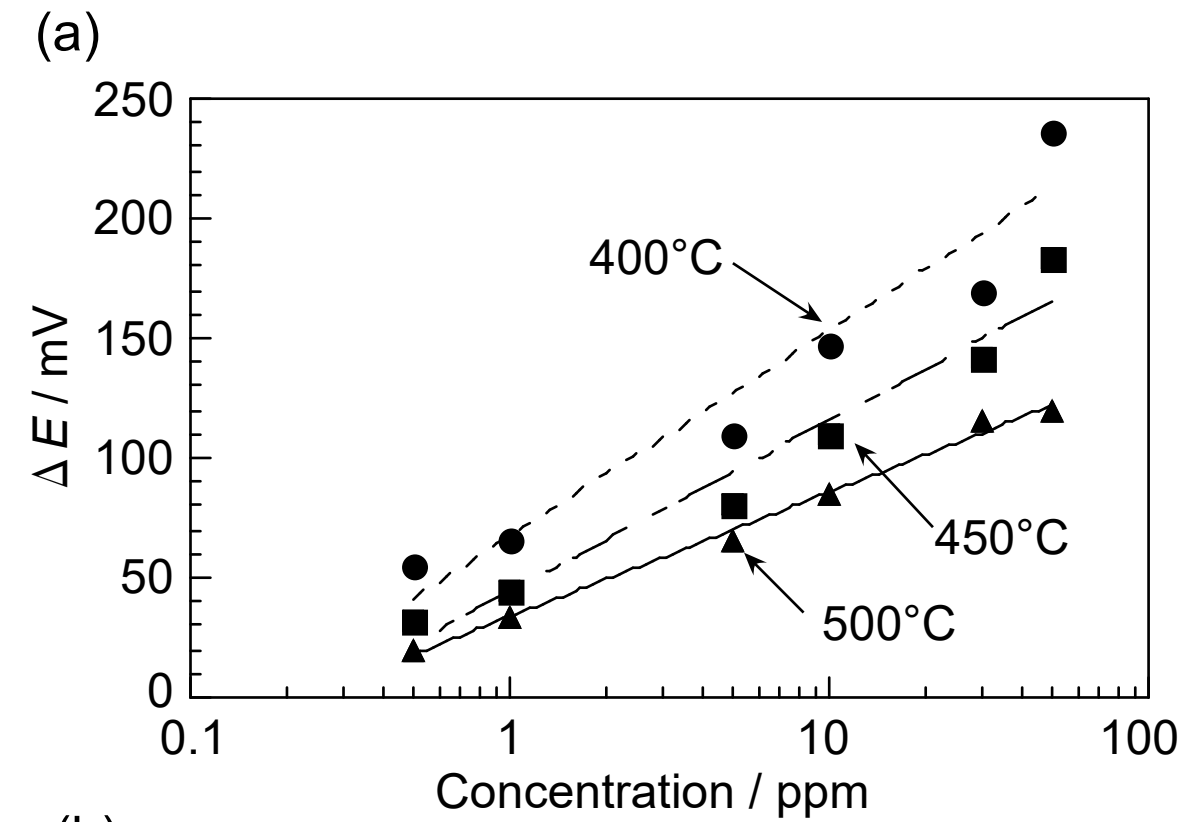


Fig. 11. Ueda et al.

## ***Biographies***

**Taro Ueda** received his B.Eng. degree in materials science and M.Eng. degree in materials science in 2003 and 2005, respectively from Kyushu Institute of Technology, and Dr.Eng. degree in 2008 from Kyushu University. He has been an assistant professor at Nagasaki University since 2013. His current research interest is the development of high-performance chemical sensors and the elucidation of gas reaction mechanism on the sensing materials.

**Hironari Abe** received his B.Eng. degree and M.Eng. degree in materials science and engineering from Nagasaki University in 2014 and 2016, respectively.

**Kai Kamada** received his B.Eng., M.Eng., and D.Eng. degrees in applied chemistry in 1997, 1999, and 2003, respectively, from Kumamoto University. He has been an associate professor at Nagasaki University since 2012. His research interests are fabrication and functionalization of various types of inorganic-bio nanohybrid materials.

**Sean R. Bishop** received his B.S. (New Mexico Institute of Technology, USA, 2003), M.S. (University of Florida, USA, 2006), and Ph.D (University of Florida, USA, 2009). Prior to his current appointment as a Senior Materials Engineer at Redox Power Systems, LLC., Sean was a research faculty at Kyushu University in Japan, investigating the coupling of electrical and mechanical properties with composition, known as electrochemomechanics in ceramic materials.

**Harry L. Tuller** received his S.B. and S.M. degrees in electrical engineering and his EngScD in solid state science and engineering from Columbia University in New York. He is a Professor in the Department of Materials Science and Engineering at MIT with current research on the integration of sensor and actuator materials into microelectromechanical (MEMS) and the modeling, processing, characterization and optimization of solid state ionic devices (sensors, batteries, fuel cells). He has published over 455 articles, coedited 15 books and been awarded 29 patents. Dr. Tuller is editor-in-chief of the Journal of Electroceramics, Springer-Nature Publishers, a fellow of the American Ceramic and Electrochemical Societies, recipient of Fulbright and von Humboldt Awards. and honorary doctorates from the University of Provence, Marseilles, France and the University of Oulu, Finland. Dr. Tuller was co-founder of Boston MicroSystems Inc., a pioneer in the design and fabrication of harsh environment

compatible micromachined SiC-based sensor arrays and is now serving as President of the International Society of Solid State Ionics (2015-17).

**Takeo Hyodo** received his B.Eng. degree in applied chemistry and M.Eng. degree in materials science and technology in 1992 and 1994, respectively, and Dr.Eng. degree in 1997 from Kyushu University. He has been an associate professor at Nagasaki University since 2010. His research interests are development of various electrochemical devices such as chemical sensors and secondary lithium-ion batteries, and design of the related mesoporous and macroporous materials.

**Yasuhiro Shimizu** received his B.Eng. degree in applied chemistry in 1980 and Dr.Eng. degree in 1987 from Kyushu University. He has been a professor at Nagasaki University since 2005. His current research concentrates on development of gas sensors based on various kinds of sensing principles.